Supporting Information

Nanofluidic Ion Regulation Membranes Based on Two-dimensional Vacancies Resided $CdPS_3$ Membrane

Meng Zhang,[‡a] Chenhui Huang,[‡a] Zhaofeng Zhai,[b] Xiaomin Kang,[a] Jiang Ju*[c] and Xitang Qian*[d]

[a] College of Mechanical Engineering, University of South China, Hengyang 421001, P. R. China

[b] Institute of Metal Research, Chinese Academy of Sciences, Shenyang, 110012, P. R. China

[c] Center for Advanced Nuclear Safety and Sustainable Development, City University of Hong Kong, Hong Kong 999077, P. R. China

[d] Department of Chemical and Biological Engineering, The Hong Kong University of Science and Technology, Kowloon, Hong Kong, P. R. China

‡ There authors contribute equally to this work.

* Corresponding author emails: Xitang Qian xtqian@ust.hk and Jiang Ju Jiang.Ju@cityu.edu.hk

Figures

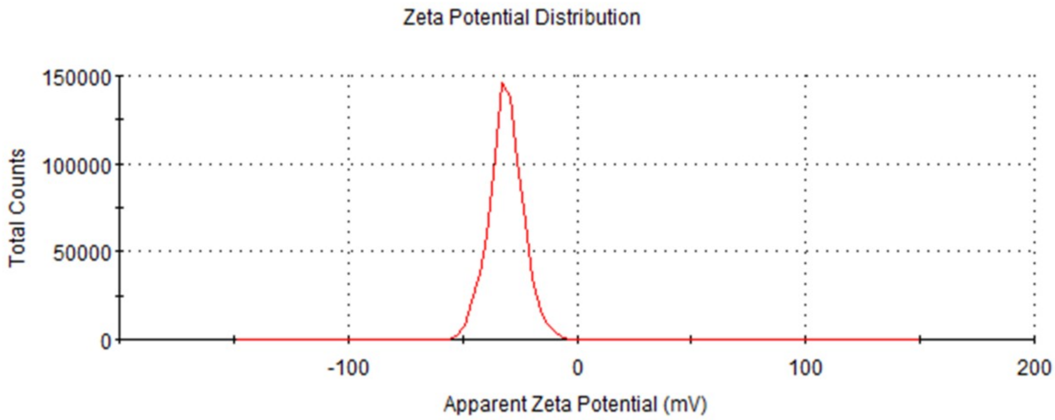

Fig. S1. The zeta potential diagram of $CdPS_3Li$ nanosheet dispersion.

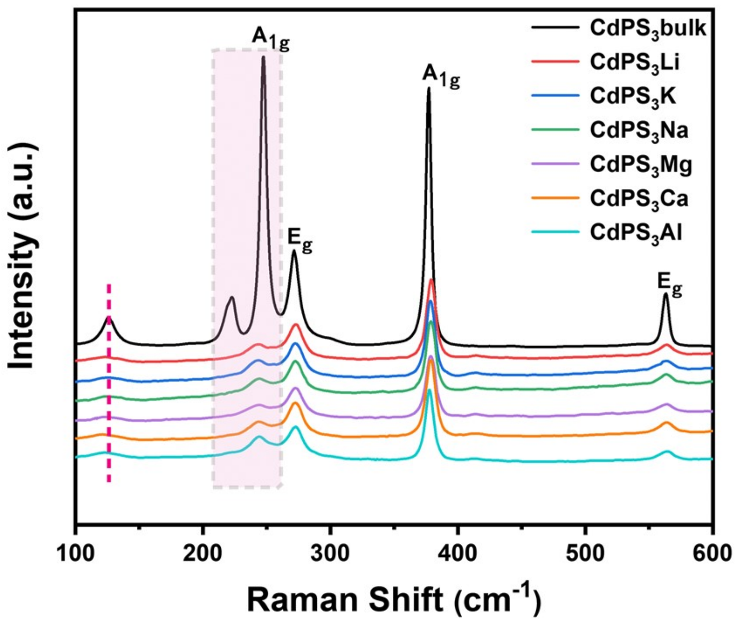

Fig. S2. Raman spectra of bulk $CdPS_3$ and $CdPS_3X$.The out-of-plane vibrations of the P_2S_6 solid exhibit the opposite motion characteristic of the $S_3P\text{-}PS_3$ unit, as discerned from the strongly polarized A1g mode that appears at 378 cm^{-1}. The Raman spectral peak at 247 cm^{-1} also confirms the significant mode caused by the symmetric stretching vibration of the P-S bond. However, those peaks appearing at 271 and 562 cm^{-1} represent in-plane vibrations in response to the $S_3P\text{-}PS_3$ unit, exemplified by the E_g mode [1].

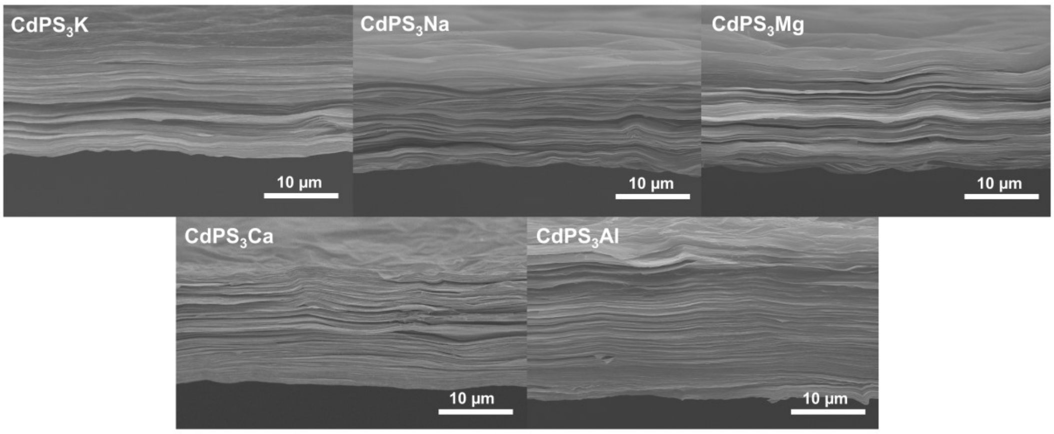

Fig. S3. Structure characterizations of $CdPS_3X$ membranes, showing well-ordered lamellar structures.

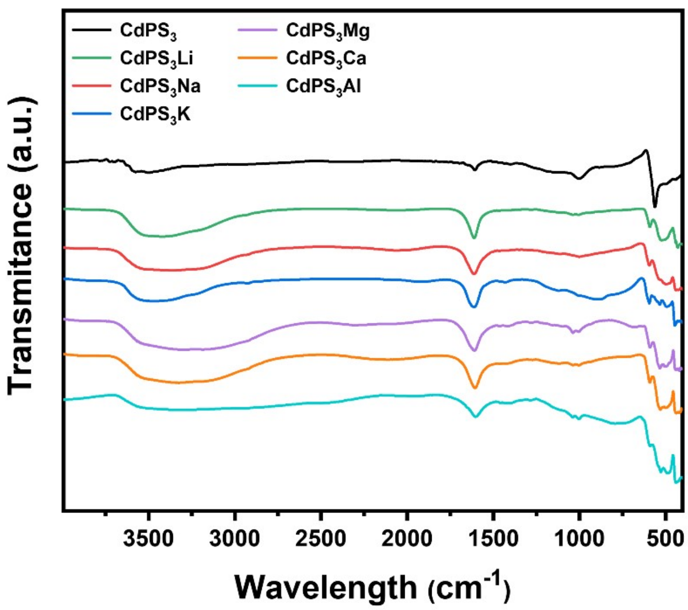

Fig. S4. FTIR spectra of bulk $CdPS_3$ and $CdPS_3X$.

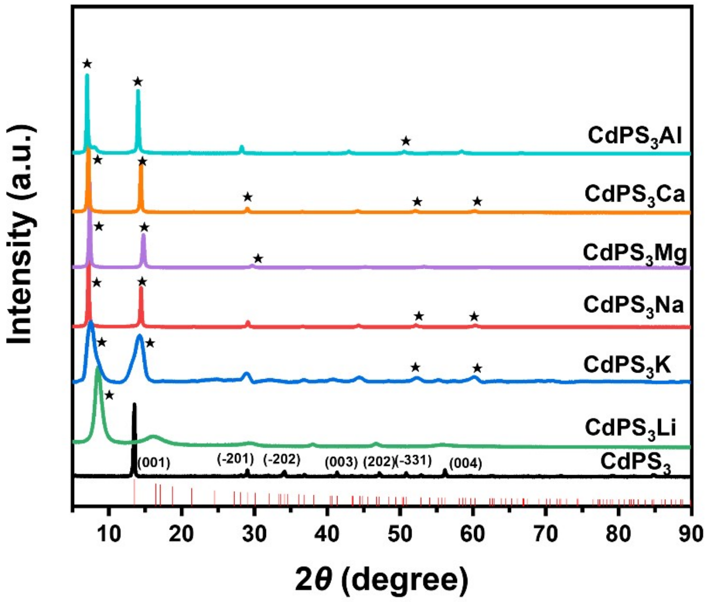

Fig. S5. XRD patterns of bulk $CdPS_3$ and $CdPS_3X$. The theoretical X-ray diffraction spectrum of the bulk $CdPS_3$ is shown as a vertical line in the figure, the star represents the multilevel diffraction peak.

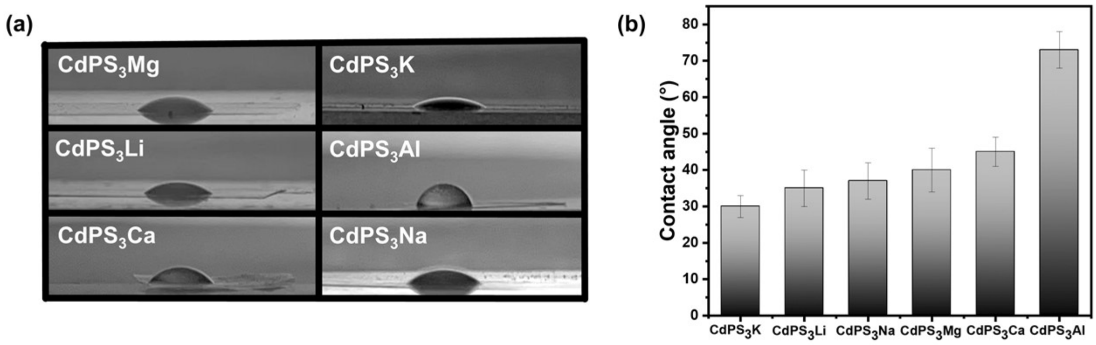

Fig. S6. (a) Contact angles of $CdPS_3X$ membranes towards water. (b) Wettability of $CdPS_3X$ membranes toward water.

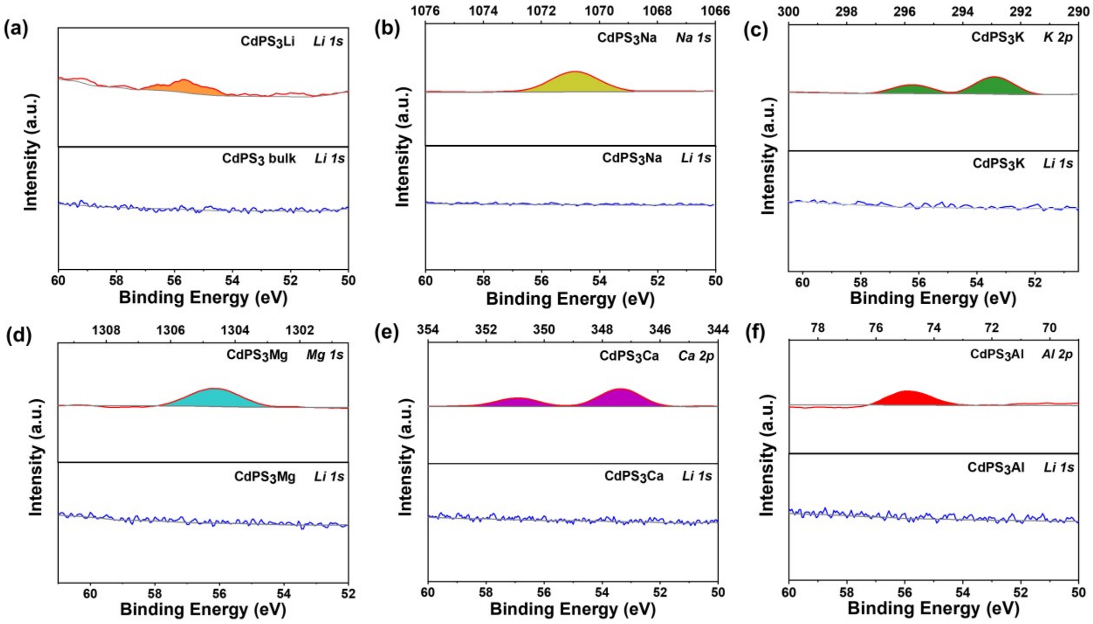

Fig. S7. XPS spectra of $CdPS_3X$ membranes. a-f, (a) Li *1s* orbitals in bulk $CdPS_3$ and $CdPS_3Li$ film. (b) Na *1s* orbitals and Li *1s* orbitals in the $CdPS_3Na$ film. (c) K *2p* orbitals and Li*1s* orbitals in the $CdPS_3K$ film. (d) Mg *1s* orbitals and Li *1s* orbitals in the $CdPS_3Mg$ film. (e) Ca *2p* orbitals and Li *1s* orbitals in the $CdPS_3Ca$ film. (f) Al *2p* orbitals and Li *1s* orbitals in the $CdPS_3Al$ film.

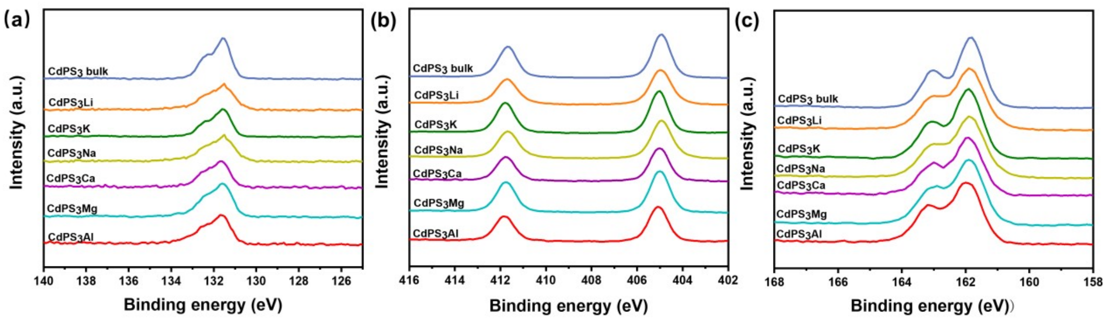

Fig. S8. XPS spectra of vc-$CdPS_3$ membranes. **a-c**, P 2*p* (a), Cd 3*d* (b), and S 2*p* (c) XPS spectra of $CdPS_3X$ membranes, which show that the valence states of P, Cd and S (+4, +2 and -2, respectively) remain the same in all the membranes.

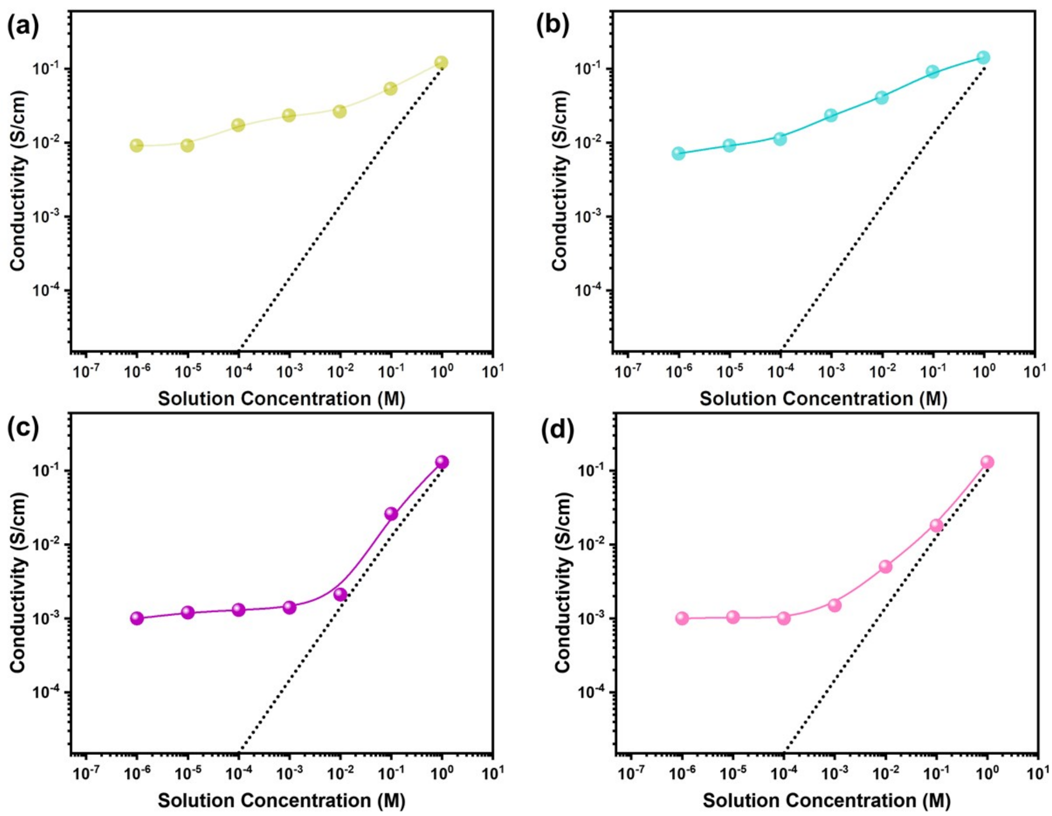

Fig. S9. (a) Ionic conductivity of $CdPS_3Na$ membrane in NaCl solution. (b) Ionic conductivity of $CdPS_3Mg$ membrane under $MgCl_2$ solution. (c)Ionic conductivity of $CdPS_3Ca$ membrane under calcium chloride solution. (d)Ionic conductivity of $CdPS_3Al$ membrane under aluminum chloride solution. The gray dashed lines represent the bulk conductivity of the corresponding salt solutions.

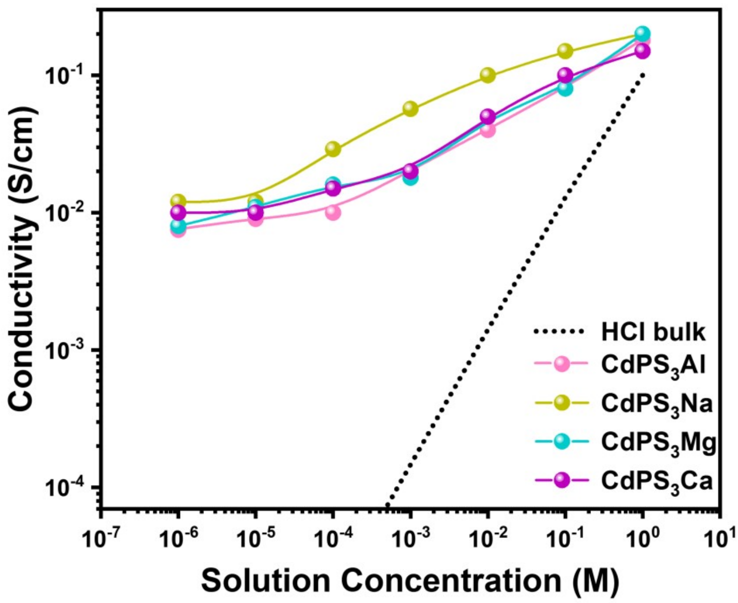

Fig. S10. Ionic conductivity in $CdPS_3X$ membranes at various HCl concentrations.The gray dashed lines represent the bulk conductivity of HCl solutions.

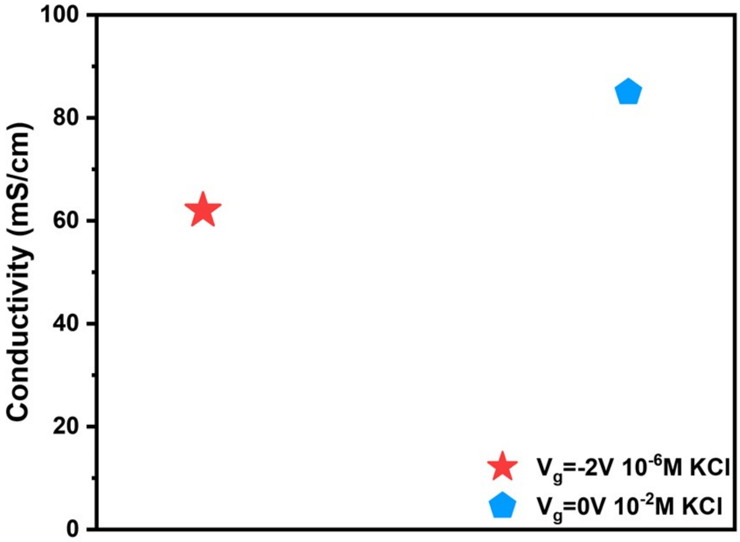

Fig. S11. Comparison of conductivity of $CdPS_3K$ membrane at different Vg.

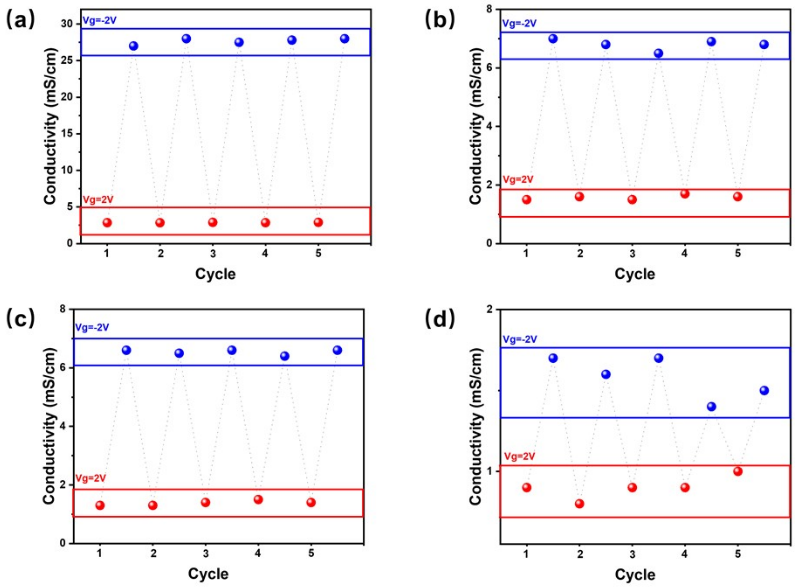

Fig. S12. (a) Plot of ions passing through $CdPS_3Na$ nanochannels as a function of time in 10^{-6} M NaCl at different Vg. (b)Plot of ions passing through $CdPS_3Mg$ nanochannels as a Function of time in 10^{-6} M $MgCl_2$ at different Vg. (c)Plot of ions passing through $CdPS_3Ca$ nanochannels as a function of time in 10^{-6} M $CaCl_2$ at different Vg. (d)Plot of ions passing through $CdPS_3Al$ nanochannels as a function of time in 10^{-6} M $AlCl_3$ at different Vg.

Tables

Material	Electrolyte	Conductivity (mS cm^{-1})	Ref.
BN	KCl solution	0.086	2
Ti_3C_2	KCl solution	0.039	3
GO	KCl solution	1	4
Cellulose	KCl solution	2	5
MXene	KCl solution	0.16	6
Elastic Wood	KCl solution	0.5	7
Montmorillonite	KCl solution	0.8	8
SLMO	KCl solution	0.6	9
$CdPS_3K$	KCl solution	10	This work

Table. S1. Comparison of ionic conductivity of different materials under 10^{-6}M KCl solution (Platform conductivity).

Material	**Electrolyte**	**Conductivity ($mS\ cm^{-1}$)**	**Ref.**
BN	KOH solution	0.037	2
MoS_2	KOH solution	0.3	10
Graphite-NFC	KOH solution	1	11
MXene	KOH solution	1.2	6
$CdPS_3K$	KOH solution	20	This work

Table. S2. Comparison of ionic conductivity of different materials under 10^{-6}M KOH solution (Platform conductivity).

Material	Electrolyte	Conductivity (mS cm^{-1})	Ref.
BN	HCl solution	0.6	2
MXene	HCl solution	1	6
Montmorillonite	HCl solution	1.4	8
GO	HCl solution	2.5	4
Graphite-NFC	HCl solution	3	11
LGM	HCl solution	4.5	12
Vermiculite	HCl solution	5.6	13
HA-GO	HCl solution	7	14
SLMO	HCl solution	10	9
$CdPS_3Al$	HCl solution	7.5	This work
$CdPS_3Ca$	HCl solution	8	This work
$CdPS_3Mg$	HCl solution	10	This work
$CdPS_3Na$	HCl solution	12	This work
$CdPS_3K$	HCl solution	23	This work

Table. S3. Comparison of ionic conductivity of different materials under 10^{-6}M HCl solution (Platform conductivity).

Material	**Electrolyte**	**Conductivity ($mS\ cm^{-1}$)**	**Ref.**
BN	NaCl solution	0.07	2
Ti_3C_2	NaCl solution	0.032	3
Graphite-NFC	NaCl solution	1	11
BN-NFC	NaCl solution	0.18	15
SLMO	NaCl solution	0.2	9
$CdPS_3Na$	NaCl solution	9	This work

Table. S4. Comparison of ionic conductivity of different materials under 10^{-6} M NaCl solution (Platform conductivity).

Material	Electrolyte	Conductivity (mS cm^{-1})	Ref.
BN	$CaCl_2$ solution	0.035	2
GO	$CaCl_2$ solution	0.6	4
$CdPS_3Ca$	$CaCl_2$ solution	1	This work
Ti_3C_2	$AlCl_3$ solution	0.067	3
$CdPS_3Al$	$AlCl_3$ solution	1	This work
$CdPS_3Mg$	$MgCl_2$ solution	6	This work

Table. S5. Comparison of ionic conductivity of different materials in 10^{-6} M $CaCl_2$, $MgCl_2$, and $AlCl_3$ solutions (Platform conductivity).

References

1. M. Naguib, M. Kurtoglu, V. Presser, J. Lu, J. Niu, M. Heon, L. Hultman, Y. Gogotsi and M. W. Barsoum, *Advanced Materials*, 2011, 23, 4248-4253.
2. S. Qin, D. Liu, G. Wang, D. Portehault, C. J. Garvey, Y. Gogotsi, W. Lei and Y. Chen, *Journal of the American Chemical Society*, 2017, 139, 6314-6320.
3. J. Lao, R. Lv, J. Gao, A. Wang, J. Wu and J. Luo, *Acs Nano*, 2018, 12, 12464-12471.
4. K. Raidongia and J. Huang, *Journal of the American Chemical Society*, 2012, 134, 16528-16531.
5. T. Li, S. X. Li, W. Kong, C. Chen, E. Hitz, C. Jia, J. Dai, X. Zhang, R. Briber, Z. Siwy, M. Reed and L. Hu, *Science Advances*, 2019, 5.

6. Y. Wang, H. Zhang, Y. Kang, Y. Zhu, G. P. Simon and H. Wang, *Acs Nano*, 2019, 13, 11793-11799.
7. C. Chen, J. Song, J. Cheng, Z. Pang, W. Gan, G. Chen, Y. Kuang, H. Huang, U. Ray, T. Li and L. Hu, *Acs Nano*, 2020, 14, 16723-16734.
8. M.-L. Liu, M. Huang, L.-Y. Tian, L. H. Zhao, B. Ding, D. B. Kong, Q.-H. Yang and J.-J. Shao, *Acs Applied Materials & Interfaces*, 2019, 11, 6665-6665.
9. H. Jin, J. Li, Z. Xu, Z. Hu, K. Liu, K. Liu, J. Duan, B. Hu, L. Huang and J. Zhou, *Science China-Materials*, 2022, 65, 2578-2584.
10. J. Park, S. Bhoyate, Y.-H. Kim, Y.-M. Kim, Y. H. Lee, P. Conlin, K. Cho and W. Choi, *Acs Nano*, 2021, 15, 12267-12275.
11. Y. Zhou, C. Chen, X. Zhang, D. Liu, L. Xu, J. Dai, S.-C. Liou, Y. Wang, C. Li, H. Xie, Q. Wu, B. Foster, T. Li, R. M. Briber and L. Hu, *Journal of the American Chemical Society*, 2019, 141, 17830-17837.
12. K. Luo, T. Huang, Q. Li, J. Lao, J. Gao and Y. Tang, *Rsc Advances*, 2022, 12, 29640-29646.
13. Y. Wu, T. Zhou, Y. Wang, Y. Qian, W. Chen, C. Zhu, B. Niu, X.-Y. Kong, Y. Zhao, X. Lin, L. Jiang and L. Wen, *Nano Energy*, 2022, 92.
14. T. J. Konch, R. K. Gogoi, A. Gogoi, K. Saha, J. Deka, K. A. Reddy and K. Raidongia, *Materials Chemistry Frontiers*, 2018, 2, 1647-1654.
15. L. Yu, T. Gao, R. Mi, J. Huang, W. Kong, D. Liu, Z. Liang, D. Ye and C. Chen, *Nano Research*, 2023, 16, 7609-7617.